Report 4112

NAVAL SHIP
RESEARCH AND DEVELOPMENT CENTER

Bethesda, Md. 20084

NUMERICAL SOLUTION OF SUBCRITICAL FLOW PAST AIRFOILS

by

Ernest O. Rogers

AVIATION AND SURFACE EFFECTS DEPARTMENT
RESEARCH AND DEVELOPMENT REPORT

May 1973

Report 4112

NUMERICAL SOLUTION OF SUBCRITICAL FLOW PAST AIRFOILS

The Naval Ship Research and Development Center is a U. S. Navy center for laboratory effort directed at achieving improved sea and air vehicles. It was formed in March 1967 by merging the David Taylor Model Basin at Carderock, Maryland with the Marine Engineering Laboratory at Annapolis, Maryland.

Naval Ship Research and Development Center
Bethesda, Md. 20034

MAJOR NSRDC ORGANIZATIONAL COMPONENTS

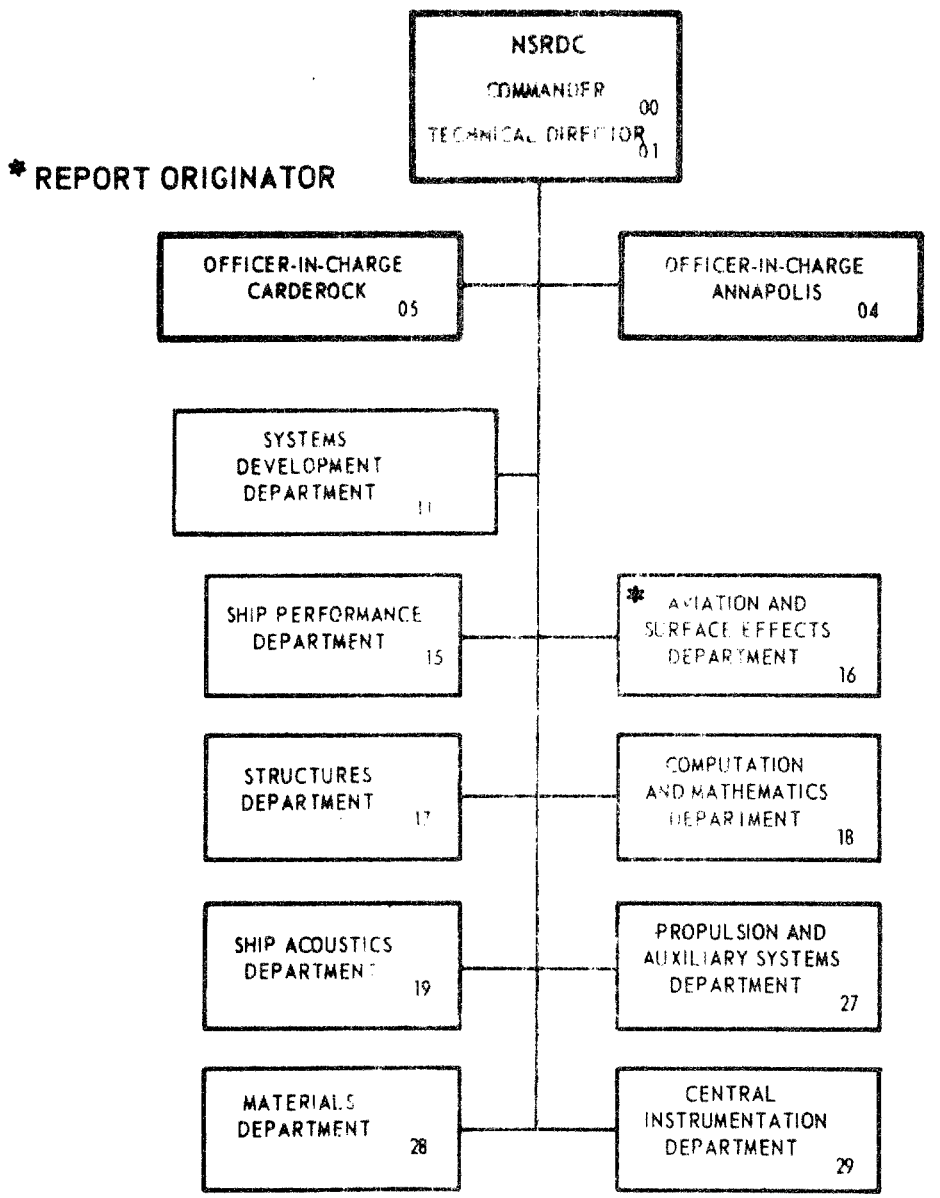

UNCLASSIFIED

SECURITY CLASSIFICATION OF THIS PAGE *(When Data Entered)*

REPORT DOCUMENTATION PAGE		READ INSTRUCTIONS BEFORE COMPLETING FORM
1. REPORT NUMBER NSRDC 4112	2. GOVT ACCESSION NO.	3. RECIPIENT'S CATALOG NUMBER
4. TITLE *(and Subtitle)* NUMERICAL SOLUTION OF SUBCRITICAL FLOW PAST AIRFOILS		5. TYPE OF REPORT & PERIOD COVERED July 1971 - April 1973 6. PERFORMING ORG. REPORT NUMBER Aero Report 1192
7. AUTHOR(s) Ernest O. Rogers		8. CONTRACT OR GRANT NUMBER(s)
9. PERFORMING ORGANIZATION NAME AND ADDRESS Aviation and Surface Effects Department Naval Ship Research and Development Center Bethesda, Maryland 20084		10. PROGRAM ELEMENT, PROJECT, TASK AREA & WORK UNIT NUMBERS Project Order 2-0127 Task Area NR 212-204 Work Unit 1-1690-111
11. CONTROLLING OFFICE NAME AND ADDRESS Office of Naval Research Code 460 Arlington, Virginia 22203		12. REPORT DATE May 1973 13. NUMBER OF PAGES 36
14. MONITORING AGENCY NAME & ADDRESS*(if different from Controlling Office)*		15. SECURITY CLASS. *(of this report)* UNCLASSIFIED 15a. DECLASSIFICATION/DOWNGRADING SCHEDULE

16. DISTRIBUTION STATEMENT *(of this Report)*

APPROVED FOR PUBLIC RELEASE: DISTRIBUTION UNLIMITED

17. DISTRIBUTION STATEMENT *(of the abstract entered in Block 20, if different from Report)*

18. SUPPLEMENTARY NOTES

Thesis topic for Master of Science Degree submitted to the Graduate School of the University of Maryland

19. KEY WORDS *(Continue on reverse side if necessary and identify by block number)*

Compressible Flow
Finite Difference
Airfoils

20. ABSTRACT *(Continue on reverse side if necessary and identify by block number)*

A finite-difference solution technique has been developed for subsonic two-dimensional inviscid flow past lifting airfoils. This work is an adaptation of the method used by Sells (1967). The full governing equations of compressible flow are written in terms of a translated velocity potential which is continuous throughout the flow field. This simplifies solutions for bluff airfoils (no Kutta condition) where both angle of attack and lift coefficient are specified. The computational plane is the interior of a unit circle obtained by mapping the flow field into the interior of the circle. A line overrelaxation matrix method is used for solution of the partial differential equation which in the iteration scheme is coupled with an algebraic equation. The numerical procedure is accurate and well behaved for all subsonic flow conditions.

DD FORM 1 JAN 73 1473 EDITION OF 1 NOV 65 IS OBSOLETE
S/N 0102-LF-014-6601

UNCLASSIFIED

SECURITY CLASSIFICATION OF THIS PAGE *(When Data Entered)*

PREFACE

This project was initiated in July 1971 and preliminary results obtained in December. The theory and numerical procedure were checked and refined by August 1972.

The author wishes to thank Dr. Walter Melnik of the University of Maryland for his encouragement and valuable advice throughout the course of this thesis project. Appreciation is also expressed to the Naval Ship Research and Development Center for use of their excellent computing facilities and to Miss Rose M. McCrossin for typing of the manuscript.

TABLE OF CONTENTS

LIST OF FIGURES

SYMBOLS

a	Local sound speed
b	$2\pi/\ell = \Delta\theta$
B	Transform modulus $\lvert dz/d\sigma \rvert$
c	$1/m = \Delta r$
c′	Chord of airfoil mapped to unit circle
C_ℓ	Section lift coefficient
C_p, CP	Pressure coefficient
C_p^*	Pressure coefficient corresponding to local speed of sound
E	Circulation constant
h_1, h_2	Curvilinear scale factors
$K(\theta), L(\theta)$	Functions in expansion of ϕ and ρ
ℓ	Number of grid lines; θ = constant
m	Number of grid lines; r = constant
M	Free-stream Mach number
M_{cr}	Critical Mach number
r	Radius, distance from center of transformed plane (circle)
$\bar{u}$	Velocity Vector
Z	Physical plane; $Z = x + iy = R_e^{i\varphi}$
α	Angle of attack
β, β_1	Constants of integration
γ	Specific heat ratio of air
Γ	Airfoil circulation
θ	Angle from trailing edge in transformed plane (circle)
θ_s	Stagnation point
ρ	Density
σ	Transformed plane; $\sigma = re^{i\varphi}$
Φ	Translated velocity potential
ϕ	Velocity potential
ψ	Stream function
ω	Relaxation parameter
Ω	Complex potential of incompressible flow

ABSTRACT

A finite-difference solution technique has been developed for subsonic two-dimensional inviscid flow past lifting airfoils. This work is an adaptation of the method used by Sells (1967). The full governing equations of compressible flow are written in terms of a translated velocity potential which is continuous throughout the flow field. This simplifies solutions for bluff airfoils (no Kutta condition) where both angle of attack and lift coefficient are specified. The computational plane is the interior of a unit circle obtained by mapping the flow field into the interior of the circle. A line overrelaxation matrix method is used for solution of the partial differential equation which in the iteration scheme is coupled with an algebraic equation. The numerical procedure is accurate and well behaved for all subsonic flow conditions.

ADMINISTRATIVE INFORMATION

The work presented herein was conducted for the Office of Naval Research (Code 460) as Project Order 2-0127, NR 212-204 and was accomplished in the time period July 1971 to April 1973.

The material was previously submitted to the University of Maryland in partial fulfillment of requirements for the degree of Master of Science, Aerospace Engineering. Thus, in some details the report deviates from the traditional format of the Naval Ship Research and Development Center (now David W. Taylor Naval Ship Research and Development Center). Preparation of this report was funded under Work Unit 1-1619-111.

INTRODUCTION

An analysis of the inviscid flow of airfoil sections is of considerable value in designing new sections and in understanding the performance of existing airfoils. Although viscous effects influence airfoil characteristics, the distribution of inviscid pressure generally agrees closely with experimental results, especially on the forward 60 to 80 percent of the airfoil. Boundary layer control techniques, which are becoming increasingly common, reduce the effects of boundary layers and thus make the inviscid condition even more applicable. Despite the usefulness of such solutions, no method has been available for an exact solution of the

governing equations of subsonic compressible flow.* The difficulty arises from the nonlinear nature of the equations.

Incompressible solutions for arbitrary airfoils have been available for many years. Until very recently, however, compressible flow solution methods have been limited to the application of so-called compressibility correction factors to the incompressible solution. The best known of these are the Prandtl-Glauert and Karman-Tsien factors that are derived from linearization of the full equations. It is generally recognized that they are adequate for flow conditions well below those that produce sonic velocity. Unfortunately, accuracy is lost as local sonic velocity is approached – just where compressibility effects are highest. The error is greatest near the leading edge where the perturbation velocities are largest and at any point where local sonic velocity is approached. This deficiency is severe enough to prohibit even an approximate determination of the critical Mach number of airfoils with rapid flow acceleration around the leading edge as on blunt-nosed, "peaky" type sections.

In 1967 Sells (Reference 1) presented a practical numerical scheme for solving the subsonic flow equations. The stream function was used as the unknown variable. Unfortunately, the behavior of the stream function at sonic velocity is such that increasingly severe numerical problems are encountered as sonic velocity is approached. Solutions are attainable up to a maximum local Mach number of about 0.95 and 0.98. Even for this, computational time becomes excessive and error develops because of the polynomial curve fit required when this approach is used.

This study originated as an attempt to avoid the limitations imposed by the stream function while retaining some of the desirable concepts used by Sells. It has led to a practical, well-behaved numerical technique for the exact solution of two-dimensional subsonic flow. This success resulted from using the velocity potential rather than the stream function.

*Shortly after this project was completed, it was learned that Garabedian and Korn of New York University were publishing a numerical technique for the compressible flow equations. Time-dependent solutions were demonstrated several years ago by Yoshihara and Magnus and others.

APPROACH

BASIC EQUATIONS*

Flow conditions will be considered as steady, inviscid, isentropic, and irrotational. The continuity equation can be expressed as

$$\nabla \cdot (\rho \cdot \bar{u}) = 0 \tag{1}$$

with the irrotationality condition given by

$$\nabla \times \bar{u} = 0 \tag{2}$$

The Bernoulli integral of the energy equation is

$$\frac{a^2}{\gamma - 1} + \frac{1}{2}\bar{u}^2 = \text{constant}$$

With

$$\rho_\infty = 1, \; |\bar{u}_\infty| = 1, \; a_\infty = 1/M$$

the isentropic relationship of

$$\frac{a^2}{a_\infty^2} = \frac{P}{P_\infty}\frac{\rho_\infty}{\rho} = \left(\frac{\rho}{\rho_\infty}\right)^{\gamma - 1}$$

can be used to give

$$a^2 = \rho^{\gamma - 1}/M^2$$

The Bernoulli equation then becomes

$$\frac{\rho^{\gamma - 1}}{(\gamma - 1)M^2} + \frac{1}{2}|\bar{u}|^2 = \frac{1}{(\gamma - 1)M^2} + \frac{1}{2} \tag{3}$$

ADVANTAGES OF THE VELOCITY POTENTIAL

The above equations imply the existence of both a velocity potential and a stream function. Equations could be written with either of these two as the unknown variable.

*The notation of Reference 1 is generally retained here for convenient comparison with the corresponding development for the stream function.

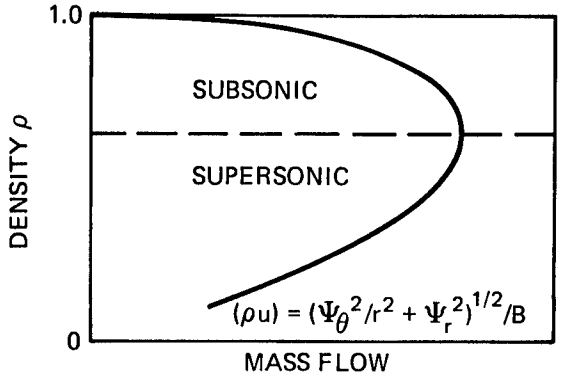

Figure 1 – Density as a Function of Mass Flow

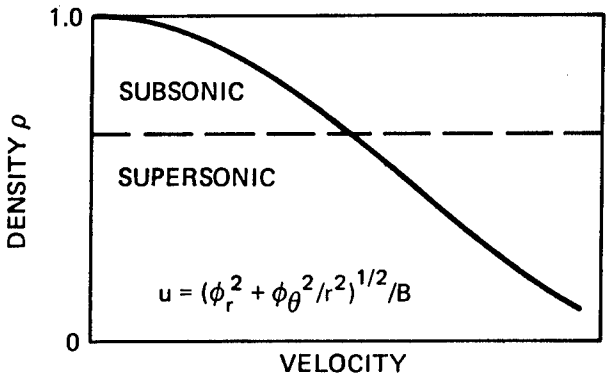

Figure 2 – Density as a Function of Velocity

As mentioned previously, the stream function is ill-behaved as local sonic velocity is approached. The nature of this problem can be seen in Figure 1. The mass flow parameter (which is associated with stream tubes) versus density relationship is multivalued with a saddle point at the speed of sound. Beginning at about M = 0.85, numerical instabilities are encountered because of the increasingly large changes in density with small changes in mass flow. Figure 2 illustrates the behavior of the velocity potential. This relationship is single valued and well-behaved. The potential is therefore to be preferred; however, it has a characteristic which must be dealt with very carefully in a numerical scheme.

There is a discontinuous change in value of the potential across a line connecting the rear stagnation point to infinity. The jump across this Kutta slice is proportional to the circulation. This can be readily handled numerically if the location of the rear stagnation point is known. From the Kutta condition, this is the trailing edge point on conventional airfoils. In recent years there has been increasing interest in airfoils with bluff trailing edges (no Kutta condition). For these sections, circulation is established and controlled by boundary layer control techniques such as tangential slot blowing over the rounded trailing edge. Analysis of the inviscid flow of such airfoils requires the specification of both angle of attack and lift coefficient. The rear stagnation point is determined as part of the solution; hence the location of the Kutta slice is not known *a priori*. This difficulty will be handled quite simply by introducing a translated potential which is continuous throughout the flow field.

NUMERICAL SOLUTION TECHNIQUE

To minimize the complexity of the finite difference solution that must be performed, the flow equations are written in the form of a partial differential equation (PDE) coupled

with an algebraic expression. In the iteration scheme, line overrelaxation matrix methods are used to solve the continuity PDE for ϕ while the density field is held constant. Then the density at all grid points is recalculated from the Bernoulli equation by using the new value of ϕ. This process is repeated until successive iterations produce insignificant changes in the unknown variables.

COORDINATE SYSTEM

The transformed coordinate system as used by Sells will also be applied here. This system employs conformal mapping methods such as that of Theodorsen to map the airfoil into a unit circle. The exterior (flow) field is then transformed by a 1/R function into the interior of the circle and this has several advantages. Infinity now appears at the circle center (r = 0), and that enables the entire infinite flow field to be included in the computations. A constant Δr, $\Delta\theta$ grid mesh in the working plane (Figure 3) provides convenient representation of the finite difference expressions with the airfoil surface always forming one side of an essentially rectangular computational cell. The most important feature is that this simple grid results in an inherent mesh refinement in the physical plane. This is readily apparent from Figure 3. The grid mesh is of higher density near the surface and the leading and trailing edges just where the flow gradients are largest. This ensures that the nose region is calculated properly. This has been an area of deficiency in many other attempts at fluid flow computations.

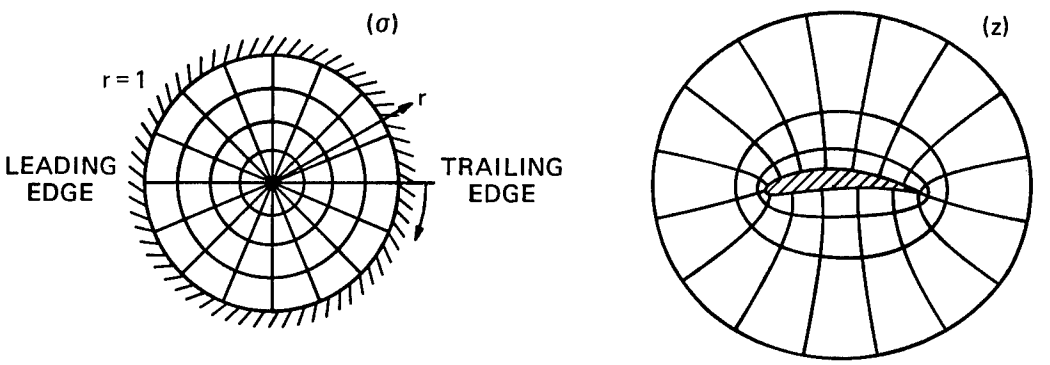

GRID IN THE COMPUTATIONAL PLANE **GRID IN THE PHYSICAL PLANE**

(From Sells, Ref. 1)

Figure 3 – Grid System

DEVELOPMENT OF EQUATIONS

EQUATIONS IN TRANSFORMED PLANE

The governing equations are now to be transformed into the unit circle coordinates r, θ by using orthogonal curvilinear coordinate system principles. Curvilinear scale factors are represented by h_1 and h_2. The element of length ds in the Z-plane is given by

$$ds^2 = |dz|^2 = h_1^2\, dr^2 + h_2^2\, d\theta^2$$

$$|dz|^2 = \left|\frac{dz}{d\sigma}\right|^2 |d\sigma|^2 = B^2 (dr^2 + r^2\, d\theta^2) \tag{4}$$

from which we find

$$h_1 = B,\ h_2 = rB \tag{5}$$

where $B(r, \theta)$ is the transform modulus $|dz/d\sigma|$ between the physical and computational planes as determined by the airfoil mapping process. The continuity equation (1) becomes

$$\frac{\partial}{\partial r}(\rho h_2 u_r) + \frac{\partial}{\partial \theta}(\rho h_1 u_\theta) = 0 \tag{6}$$

From the irrotationality condition (2)

$$\frac{\partial}{\partial r}(h_2 u_\theta) - \frac{\partial}{\partial \theta}(h_1 u_r) = 0 \tag{7}$$

there is a function $\phi(r, \theta)$ such that

$$\frac{\partial \phi}{\partial \theta} = h_2 u_\theta,\ \frac{\partial \phi}{\partial r} = h_1 u_r \tag{8}$$

Substituting (8) into (6),

$$\frac{\partial}{\partial r}\left(\rho \frac{h_2}{h_1} \phi_r\right) + \frac{\partial}{\partial \theta}\left(\rho \frac{h_1}{h_2} \phi_\theta\right) = 0 \tag{9}$$

or, from (5), the continuity equation is

$$\frac{\partial}{\partial r}\left(\rho r \frac{\partial \phi}{\partial r}\right) + \frac{\partial}{\partial \theta}\left(\frac{\rho}{r} \frac{\partial \phi}{\partial \theta}\right) = 0 \tag{10}$$

The Bernoulli equation

$$\rho = \left[1 + \frac{\gamma - 1}{2} M_\infty^2 (1 - \bar{u}^2)\right]^{1/(\gamma-1)} \tag{11}$$

remains unchanged except for the expression for velocity obtained from (5) and (8):

$$|\bar{u}|^2 = u_r^2 + u_\theta^2 = \frac{1}{B^2}\left[\frac{\partial \phi}{\partial r}^2 + \frac{1}{r^2}\frac{\partial \phi}{\partial \theta}\right]^2 \tag{12}$$

BOUNDARY CONDITIONS

At the surface, appropriate boundary conditions are no flow normal to the surface

$$u_r = 0 \tag{13}$$

and no flow around the sharp trailing edge (if there is one),

$$\phi_\theta = 0 \text{ for } \theta = 0 \tag{14}$$

The transformation procedure is assumed to map the trailing edge into the point $\theta = 0$. This boundary condition is not applied for bluff airfoils.

Conditions at infinity correspond to free-stream values with

$$\rho = \rho_\infty, \; u = u_\infty$$

The infinity condition of free-stream velocity cannot be imposed directly; what is needed is an expression for ϕ. For a first examination of ϕ at infinity, we assume that at large distances $|Z|$ in the physical plane, the density is essentially the free-stream value and therefore can be considered constant. The flow is then essentially incompressible so that we can examine the complex potential Ω for steady flow at incidence α with circulation represented by E. For large $|Z|$ (see any standard text on incompressible flow)

$$\Omega = \phi + i\psi \sim Ze^{-i\alpha} - i\,E \ln z$$

With $Z = Re^{i\varphi}$, the velocity potential can be expressed as

$$\phi = R \cos(\varphi - \alpha) + \varphi E \tag{15}$$

and with transformation into the circle by $R \sim 1/r$, $\varphi = -\theta$

$$\phi(0, \theta) \sim \frac{1}{r} \cos(\theta + \alpha) - \theta E \tag{16}$$

Thus, conditions at infinity are represented by a dipole and a vortex.

TRANSLATED POTENTIAL

The previous expression for ϕ at infinity reveals a singularity at r = 0 and a jump in ϕ at $\theta = 2\pi$. The singularity and the jump can be removed by defining a translated potential

$$\Phi(r, \theta) = \phi - \frac{1}{r} \cos(\theta + \alpha) + \theta E \tag{17}$$

This function is finite and continuous everywhere. The numerical scheme will solve for Φ, and if needed, the value of ϕ itself can of course be found from

$$\phi(r, \theta) = \Phi + \frac{1}{r} \cos(\theta + \alpha) - \theta E \tag{18}$$

The boundary condition at infinity for Φ will be found by first taking a closer look at the asymptotic behavior of ϕ.

BOUNDARY CONDITION FOR THE TRANSLATED POTENTIAL

Expanding ϕ and ρ about r = 0 to one more term, we have

$$\phi = \frac{1}{r} \cos(\theta + \alpha) - \theta E + L(\theta) + 0(r) \tag{19}$$

$$\rho = 1 + rK(\theta) + 0(r^2) \tag{20}$$

In addition it should be noted that for large $|Z|$, the nature of the transformation employed is such that (Reference 1)

$$B = \left|\frac{dz}{d\sigma}\right| = \frac{1}{r^2} \left[1 + 0(r^2)\right]$$

Substituting the above in the continuity equation (10), terms $0(1/r^2)$ cancel and terms $0(1/r)$ give

$$\frac{d}{d\theta} \left[L'(\theta) - K(\theta) \sin(\theta + \alpha)\right] = 0 \tag{21}$$

so that

$$L'(\theta) - K(\theta) \sin(\theta + \alpha) = -\beta_1 \tag{22}$$

Similarly with the expansion for ϕ and ρ substituted into the Bernoulli equation, terms $0(r)$ give

$$\frac{K(\theta)}{M^2} + E \sin(\theta + \alpha) - L' \sin(\theta + \alpha) = 0 \tag{23}$$

Equations (22) and (23) can be solved for K and L'

$$K(\theta) = \frac{(E + \beta_1) \sin(\theta + \alpha)}{\sin^2(\theta + \alpha) - \left(\frac{1}{M^2}\right)} \tag{24}$$

$$L'(\theta) = \frac{E \sin^2(\theta + \alpha) + \beta_1 \left(\frac{1}{M^2}\right)}{\sin^2(\theta + \alpha) - \left(\frac{1}{M^2}\right)} \tag{25}$$

Integration of (25) leads to

$$L(\theta) = \frac{-(E + \beta_1)}{\sqrt{1 - M^2}} \tan^{-1}\left[\sqrt{1 - M^2}\, \tan(\theta + \alpha)\right] + E(\theta + \alpha) + \beta \tag{26}$$

The additive constant β has no physical significance in the potential and can be dropped without loss of generality. From (19), (26), and (17), the boundary value of Φ becomes

$$\Phi(0, \theta) = \frac{-(E + \beta_1)}{\sqrt{1 - M^2}} \tan^{-1}\left[\sqrt{1 - M^2}\, \tan(\theta + \alpha)\right] + E(\theta + \alpha) \tag{27}$$

This asymptotic value is a function of the direction from which r = 0 is approached. The constant β_1 will be determined from the consideration that Φ be continuous with no jump at the rear stagnation point θ_s (2π for conventional airfoils). Observe that $L(\theta) \to 0$ as $M \to 0$ is also required.

CIRCULATION CONSIDERATIONS

From the definition of circulation we have

$$\Gamma = \oint u_\theta \, ds = \int_{\theta_s}^{\theta_s + 2\pi} \frac{1}{rB} \frac{\partial \phi}{\partial \theta} \, rB \, d\theta = \int_{\theta_s}^{\theta_s + 2\pi} \frac{\partial \phi}{\partial \theta} \, d\theta \tag{28}$$

where θ_s is the location of the rear stagnation point.

Obtaining ϕ_θ from (18), we then have

$$\Gamma = -2\pi E + \Phi(\theta_s + 2\pi) - \Phi(\theta_s) \tag{29}$$

and by using (27), one obtains

$$\Gamma = \frac{-(E+\beta_1)}{\sqrt{1-M^2}}\,2\pi \tag{30}$$

The value of β_1 remains to be found. It is desired that Φ be a continuous function which implies that

$$\oint \frac{\partial \Phi}{\partial \theta}\,d\theta = \int_{\theta_s}^{\theta_s+2\pi} \frac{\partial \Phi}{\partial \theta}\,d\theta = 0 \tag{31}$$

From this requirement

$$\beta_1 = E\left(\sqrt{1-M^2} - 1\right) \tag{32}$$

and

$$\Gamma = -2\pi E \text{ or } E = -\frac{\Gamma}{2\pi} \tag{33}$$

Finally, with these constants we obtain the boundary value of Φ

$$\Phi(r \to 0, \theta) = \frac{\Gamma}{2\pi}\left\{\tan^{-1}\left[\sqrt{1-M^2}\,\tan(\theta+\alpha)\right] - (\theta+\alpha)\right\} \tag{34}$$

The relationship between circulation and the lift coefficient C_ℓ is given by

$$L = \rho_\infty u_\infty \Gamma = C_\ell\, c'\, \frac{1}{2}\rho_\infty u_\infty^2 \tag{35}$$

where c' is the chord of the airfoil mapped to the unit circle. The result is that

$$C_\ell = \frac{-4\pi E}{c'} \tag{36}$$

or for bluff airfoils where C_ℓ is a specified condition,

$$E = \frac{-C_\ell\, c'}{4\pi} \tag{37}$$

FINAL EQUATIONS

Equations in terms of Φ are readily obtainable by substituting (18) into (10). With

$$\phi_r = -\frac{1}{r^2}\cos(\theta+\alpha) + \Phi_r$$

$$\phi_\theta = -\frac{1}{r}\sin(\theta+\alpha) - E + \Phi_\theta$$

$$\phi_{rr} = \frac{2}{r^3}\cos(\theta+\alpha) + \Phi_{rr}$$

$$\phi_{\theta\theta} = -\frac{1}{r}\cos(\theta+\alpha) + \Phi_{\theta\theta}$$

we obtain

$$\left[r^2\,\Phi_r - \cos(\theta+\alpha)\right]\rho_r - \left[\frac{1}{r}\sin(\theta+\alpha) + E - \Phi_\theta\right]\rho_\theta + \rho\left[r^2\,\Phi_{rr} + r\,\Phi_r + \Phi_{\theta\theta}\right] = 0 \tag{38}$$

This is the PDE to be solved by matrix methods while the density ρ is held constant. The density is then recalculated from the Bernoulli equation (11) by using the newly obtained values of Φ:

$$\rho = \left[1 + \frac{\gamma-1}{2}M_\infty^2\left[1 - \frac{1}{B^2}\left(\left[\Phi_r - \frac{1}{r^2}\cos(\theta+\alpha)\right]^2 + \left[\Phi_\theta - \frac{1}{r}\sin(\theta+\alpha) - E\right]^2/r^2\right)\right]\right]^{1/(\gamma-1)}$$

Surface boundary conditions become

$$\Phi_r = \cos(\theta+\alpha) \tag{39}$$

If there is a Kutta condition

$$u_\theta = -\frac{1}{B}\left[\sin(\theta+\alpha) + E - \Phi_\theta\right] = 0 \tag{40}$$

from which follows the means by which the circulation is established:

$$E = \Phi_\theta - \sin(\alpha) \tag{41}$$

For bluff airfoils, E is calculated directly from (37) by using the input C_ℓ with the rear stagnation point location found as part of the solution. Conditions at infinity are given by (27).

NUMERICAL METHODS

The complete numerical scheme is diagrammed in Figure 4. The discussion in the next two sections refer to the MATRIX SOLN block (Figure 4).

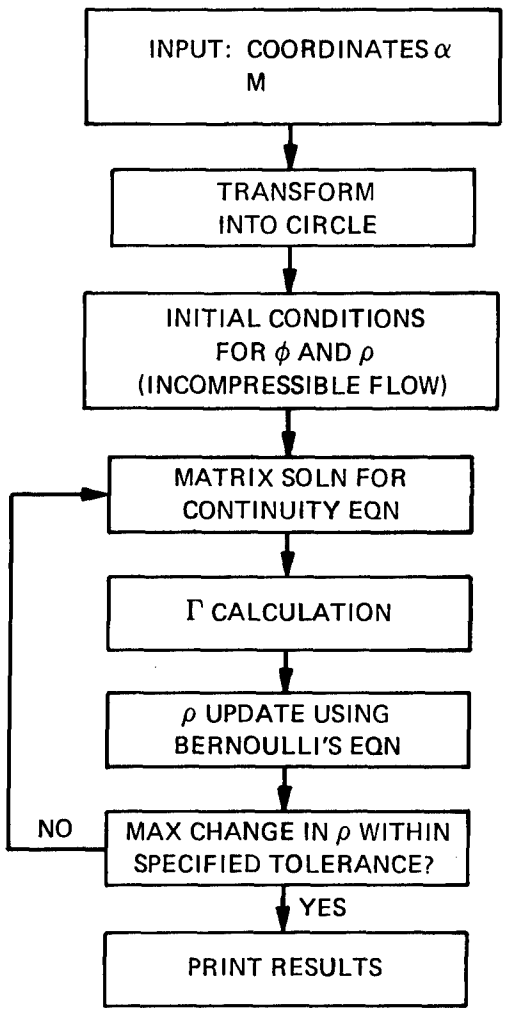

Figure 4 – Flow Diagram for Numerical Solution

FINITE DIFFERENCES

Figure 5 is a schematic of the computational grid. For each point we write the finite-difference equivalence of the derivatives in the continuity equation (38). The equation is elliptic for subcritical flow; this means that point 0 in Figure 5 is influenced by all surrounding points. The finite differencing must reflect this domain of dependence by using centered differences. Substitution of the finite-difference expressions in (38) will result in an equation

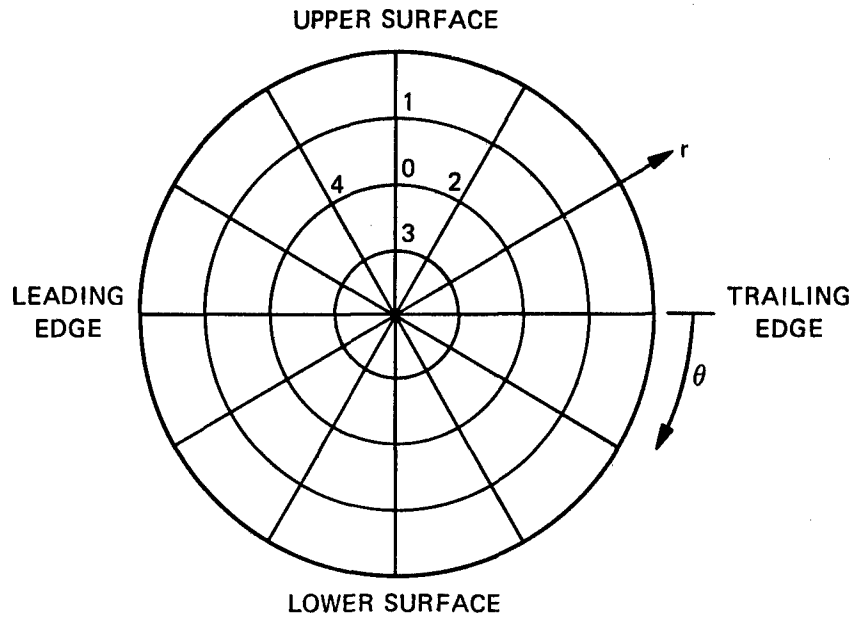

Figure 5 – Finite Difference Computational Grid

for Φ at the point 0 in terms of ρ and Φ at adjacent points. (Details of this development are given in the appendix.) This is done for each point in the field of typically 1800 points, resulting in a like number of simultaneous equations for the values of Φ.

LINE OVERRELAXATION

It is not feasible to solve the complete set of equations simultaneously. Instead an iteration scheme can be formed to enable the flow field to be solved in successive parts. Referring to Figure 5, we can use standard matrix methods to solve for Φ on successive lines – either lines of constant θ or constant r. Lines of constant r, that is concentric circles, were found to be more efficient in computer time. With an initial condition of incompressible flow, a Gauss-Seidel matrix method is used on each line starting from the innermost circle (nearly free-stream conditions) and working to the one adjacent to the surface. The values of Φ newly computed for one line are used on the line that follows, and so on. Surface values of Φ are found from the enforcement of the flow tangency condition thereby using one-sided differences (see the appendix).

Line overrelaxation was found to greatly reduce the number of iterations required. (An iteration consists of one pass through the complete computational grid to obtain new estimates of Φ followed by the recalculation of density at all points.) Overrelaxation accelerates convergence by using the difference between successive iterations to estimate a presumably

more accurate value. This is done on a line-by-line basis and is expressed by

$$\Phi_{new} = \Phi_{new}\,\omega + (1 - \omega)\,\Phi_{previous}$$

where ω is the relaxation factor. Theoretically, values approaching 2.0 can be used without instabilities developing. It was found that a factor of 1.9 produced the fastest convergence. The number of iterations for convergence is shown in Figure 6 as a function of the relaxation factor.

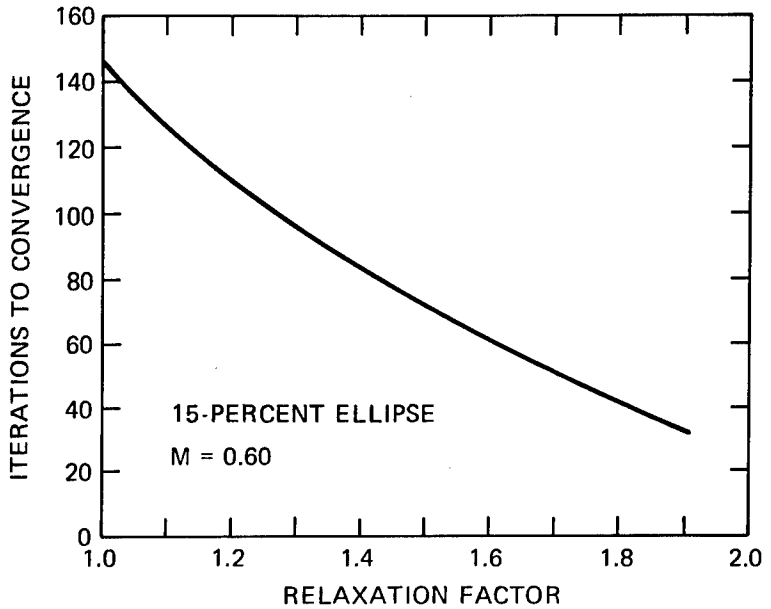

Figure 6 – Number of Required Iterations as a Function of Relaxation Factor for a Typical Case

Radial line (constant θ) relaxation was also tried. Since the boundary conditions at each end of the line are known, a simple tridiagonal matrix solution is possible. The radial line approach was found to be much less satisfactory, as will be discussed later.

CONVERGENCE

The overall numerical scheme has been diagrammed in Figure 4. After a pass through the field to calculate new values of Φ, the density at each point is updated by using the Bernoulli equation. Circulation is recalculated before the density calculation. Then another pass is made for Φ. When the density is updated at each point, the extent of change from the previous value is checked. When this difference, or residual, is below a specified level, convergence is considered complete. It was found that a density change of 0.25×10^{-4}

(normalized to free-stream density) gave sufficient accuracy for practical applications. Figure 7 shows how the number of iterations required for a given residual varies for a typical case. Residuals of circulation or Φ could also be used as convergence criteria; however, they were not tried here.

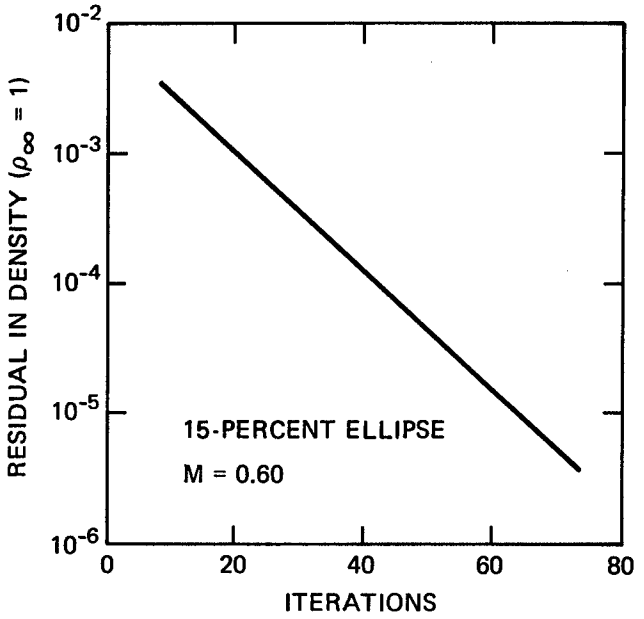

Figure 7 – Residual Reduction with Increasing Iteration for a Typical Case

COMPUTATIONAL ASPECTS

It was found that time per iteration on the CDC 6600 computer can be expressed by

$$T \text{ (sec/iteration)} = 0.24 (\ell m) \times 10^{-3}$$

where ℓ is the number of radial lines and m the number of concentric circles or increments in θ and r, respectively. The number of iterations required for convergence in a given case appeared to be linearly proportional to m; thus the total time for a solution is proportional to ℓm^2.

The mesh size required to obtain a given accuracy depends on the gradients of the dependent variable. The grid selected as the best compromise between computational costs and accuracy was ℓ = 120, m = 15. If the pressure distribution is smooth ("non-peaky") then a grid of 120 x 10 is acceptable. For peaky, high-leading-edge acceleration profiles, a grid of 160 x 15 is recommended.

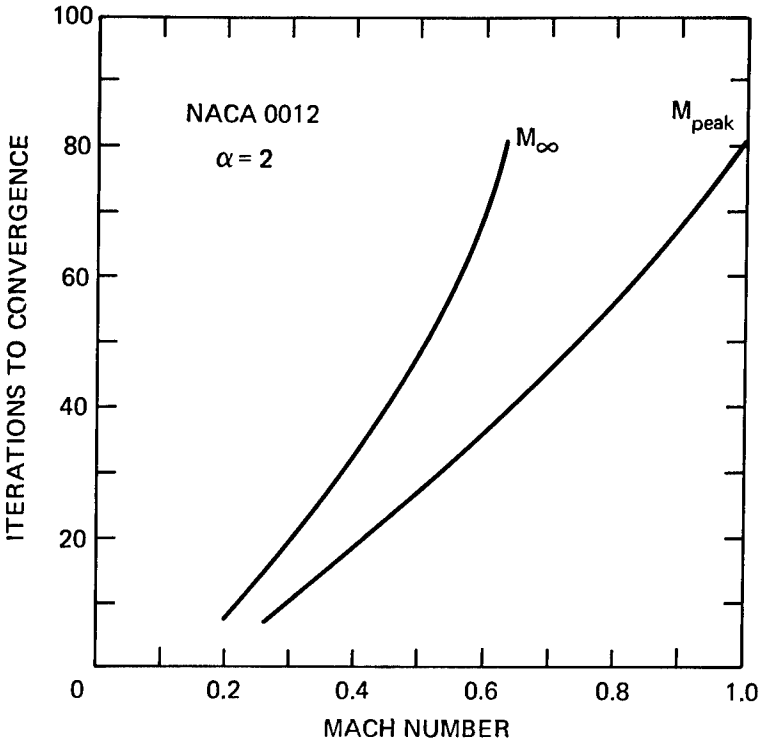

Figure 8 – Variation of Number of Iterations with Mach Number for a Typical Case

The total number of iterations is also a function of the extent of compressibility effects which are proportional to the free-stream Mach number and the peak surface velocity. Figure 8 illustrates the variation of number of iterations with Mach number for a typical case.

The above discussion applies to the initial conditions corresponding to incompressible flow. If, for example, several Mach numbers are to be run for a given configuration, then the converged solution can be used as the starting condition for the next Mach number. The number of iterations required is thus substantially reduced. This technique offers one way of checking the degree of convergence. This is done by computing the same case by starting from converged solutions below and above the free-stream Mach number of interest.

As mentioned previously, radial line overrelaxation was also investigated. At first this was tried by starting at $\theta = 0$ and moving in a clockwise direction (Figure 5). The relaxation factor that gave the fastest convergence was 1.6. It was found that the converged solution differed slightly from the concentric circle solution. Closer observation of flow over symmetrical airfoils indicated a dissymmetry in the pressure distribution. For example, the location of the suction peak was shifted forward on the lower surface and rearward on the upper surface. Reversing the direction of line overrelaxation to counterclockwise reversed the dissymmetry. If the converged concentric circle solution is utilized as the initial condition,

it satisfies the radial line version immediately without further iteration; if the converged solution of a radial line solution is used as the initial condition, it too satisfies the matrix. Therefore two significantly different results would satisfy the radial line matrix scheme. As a further experiment, it was found that if a radial line solution was used as input to the concentric circle version, several iterations were required before convergence was attained. The resulting solution was the same as that produced by starting from incompressible conditions.

Alternating sweep direction from one iteration to the next was also tried. Convergence was slow and unsteady, but the solution was found to be more nearly like that of the concentric circle matrix.

This distortion in the radial line solution was considered attributable to use of the updated Φ from the previous line. Use of the old value of Φ failed to produce convergence, but when the program was terminated, the pressure distribution was found to be undistorted. As a check on the programming, the converged solution from the concentric circle matrix was used as the initial condition. Convergence was immediate.

Reversed direction for the concentric circle method was also tried. This consisted of moving from the outer circle to the center of the working plane rather than the other way. More iterations were required for convergence, but the solution was the same as for the other direction. In addition, multiple passes through the matrix solution before density update were tried, but these offered no advantages in computational time.

RESULTS

The computer program of Reference 2 was used to transform airfoils into the circle. For circular and elliptical sections, the transformation was performed analytically.

VERIFICATION

Validation of this numerical method is hampered by the limited number of accurate solutions that are available for comparison purposes. The critical Mach number (M_{cr}) of a circular cylinder has been expressed analytically as a series summation. Although this series has not been completely evaluated, the circle was selected as a check case.

For the utmost accuracy, a grid of 240 x 30 was used and the free-stream Mach number was increased incrementally until local sonic velocity was reached. Critical Mach number (0.3985) is in agreement with the value reported in Reference 3. The pressure distribution is shown in Figure 9. A more practical grid size of 160 x 15 gave a result of 0.3990.

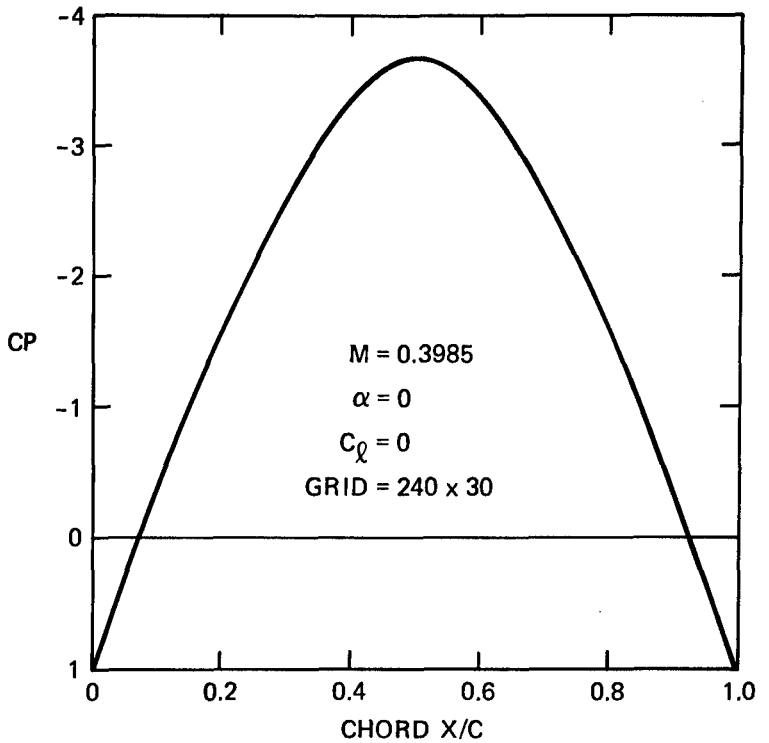

Figure 9 – Pressure Distribution on Circular Cylinder at the Critical Mach Number of 0.3985

As a check on the treatment of circulation, the lift coefficient was found for a circle at which the two stagnation points merged and began to leave the surface. This value of 13.2 (Figure 10) is in the range expected from incompressible flow theory. The critical value for this condition was used, namely, Mach = 0.19. As a further test, a value of 20.0 was specified for C_ℓ. As expected, the stagnation points had left the surface and were found in the flow field. The entire surface flow was moving in the same direction (Figure 11). No numerical instabilities were encountered.

Numerical hodograph methods have been developed that give a precise (within numerical error) relationship between pressure and airfoil geometry for the design Mach number. A design with a peak Mach number of 0.982 was selected from Reference 4. The agreement is shown in Figure 12.

No lifting hodograph designs were available for a check of lifting flow. However, a rough check is possible by determining how C_ℓ varies with Mach number for a fixed angle of attack. It is known that as a first approximation, the variation is according to the Prandtl-Glauert factor. The results for an NACA 0012 section at $\alpha = 2.0$ are shown in Figure 13. The general trend matches the $\sqrt{1 - M^2}$ variation.

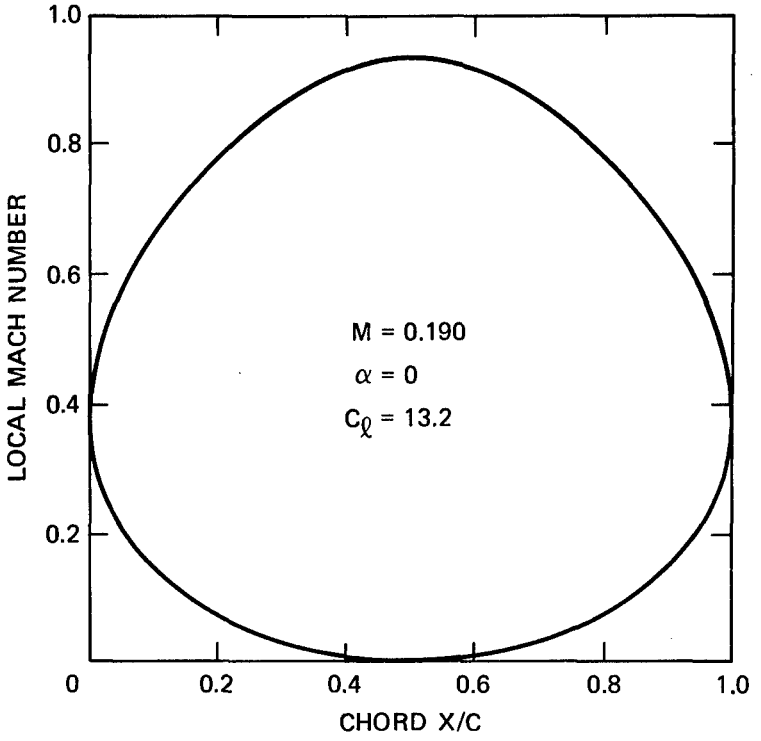

Figure 10 – Mach Number Distribution on Circular Cylinder for Nearly Critical Flow and Circulation Corresponding to Merged Stagnation Points

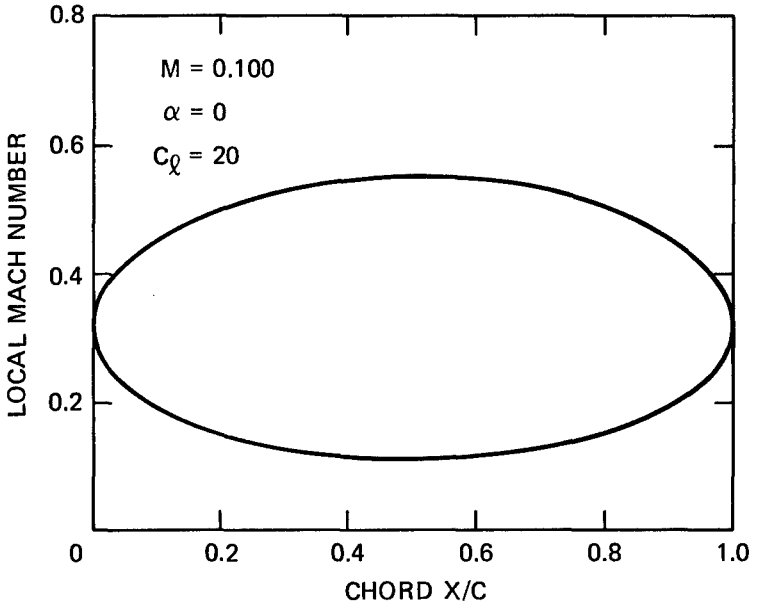

Figure 11 – Mach Number Distribution on Circular Cylinder for a Specified Lift Coefficient (Note that the stagnation point has left the surface)

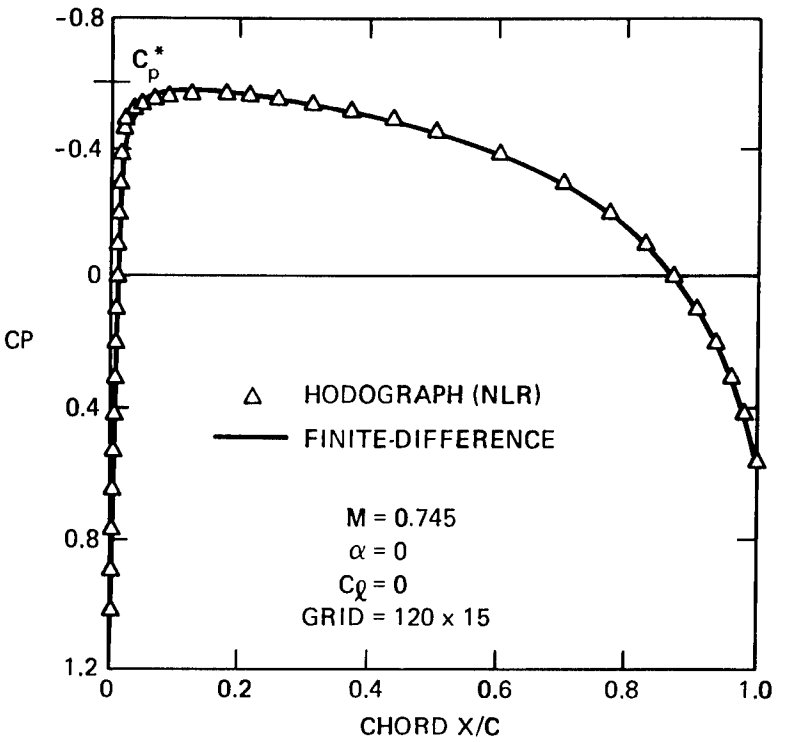

Figure 12 – Comparison of Finite-Difference Solution with Hodograph-Designed Airfoil

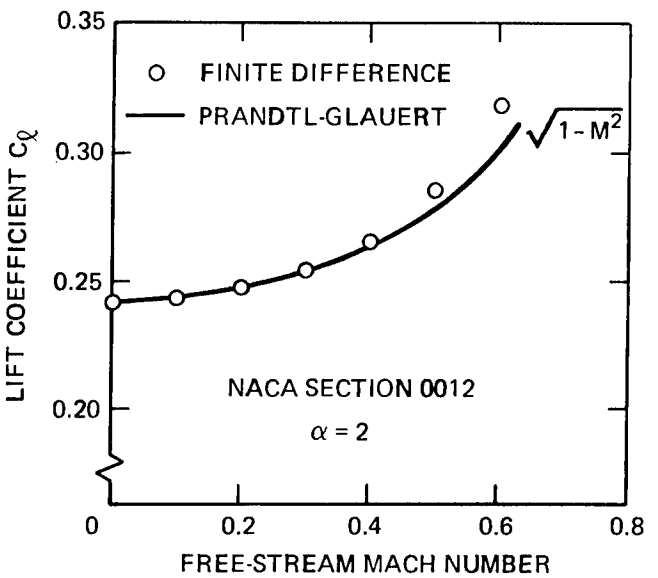

Figure 13 – Variation of Lift Coefficient with Mach Number

Within the computer program itself, lift can be checked by comparing the lift coefficient obtained from the calculated circulation with that obtained from numerical integration of the pressure distribution. In nearly all cases, the difference in the two C_ℓ values was less than 0.2 percent and usually about 0.1 percent. This is an order of magnitude better than obtained by using the stream function (Reference 1).

COMPARISON WITH OTHER METHODS

It is of considerable interest to compare results obtained by compressibility factor methods with those of the present exact numerical solution. The Prandtl-Glauert factor is given by

$$C_P = C_{P_{inc}} / \sqrt{1 - M^2}$$

while the Karman-Tsien factor is

$$C_P = C_{P_{inc}} / (\sqrt{1 - M^2} + 0.5\, C_{P_{inc}} (1 - \sqrt{1 - M^2}))$$

where $C_{P_{inc}}$ is the incompressible value of the local pressure coefficient and M is the free-stream Mach number.

Figure 14 compares the determinations of pressure distribution for a 15-percent-thick ellipse at nearly critical Mach number. Note that both compressibility factors overpredict the nose and underpredict the midchord suction. Also note the difference in the shapes of the curves. The correction factor technique will always give a curve which closely resembles the shape of the incompressible distribution. However, the exact solution will give a curve which changes overall shape rapidly as the critical Mach number is approached.

The overprediction of leading edge suction is characteristic of the correction factors and worsens for sections with blunt leading edges that result in faster flow acceleration. The hodograph airfoil is compared with the Karman-Tsien factor in Figure 15. The large discrepancy at the nose would result in a very erroneous prediction of M_{cr} for this airfoil. (Actually, the Karman-Tsien method would indicate supersonic flow; in practice, therefore, the results would be discarded for this Mach number.) This difference is a strong function of peak Mach number. Figure 16 compares the Karman-Tsien method with present results for a 15-percent ellipse with a rounded leading edge at two Mach numbers. Once again there is a large discrepancy at high subsonic velocities (Figure 16a). For a substantially lower free-stream velocity, however, the Karman-Tsien approach gives an acceptable solution (Figure 16b). It should be pointed out that the sonic velocity for lifting cases can be reached for free-stream Mach numbers of 0.3 or lower.

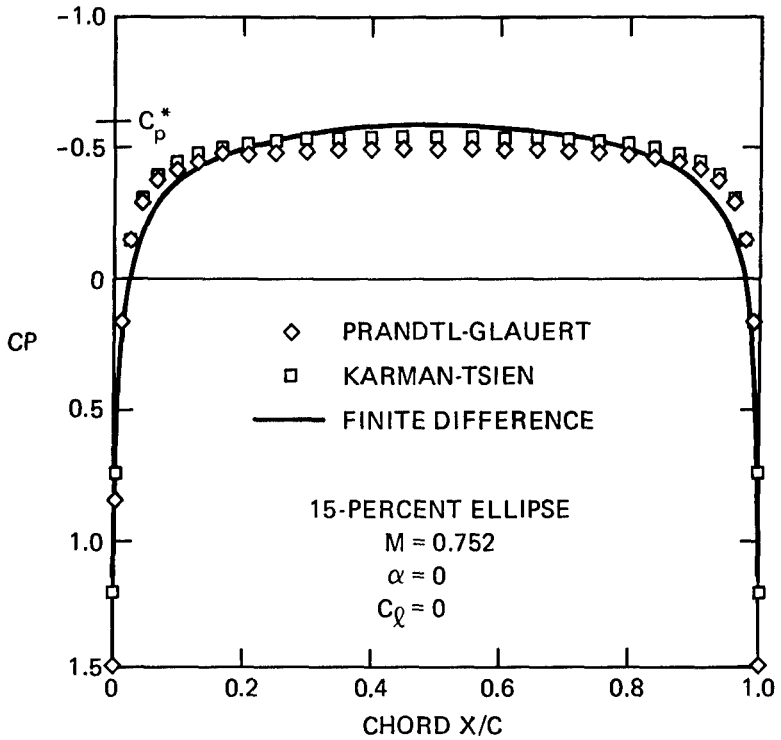

Figure 14 – Comparison of Present Method with Prandtl-Glauert and Karman-Tsien Correction Factors

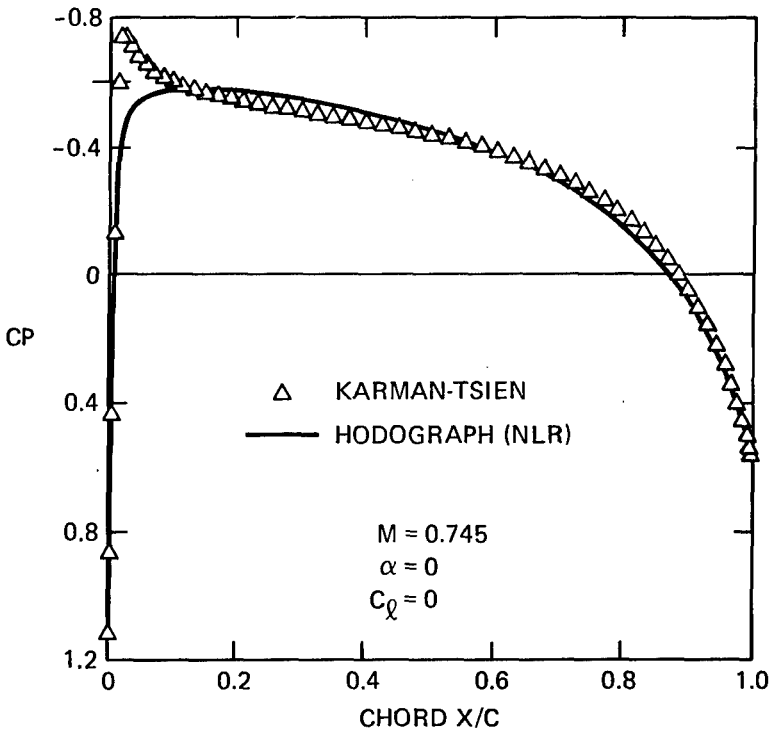

Figure 15 – Comparison of Karman-Tsien Method with Hodograph Solution of Figure 12

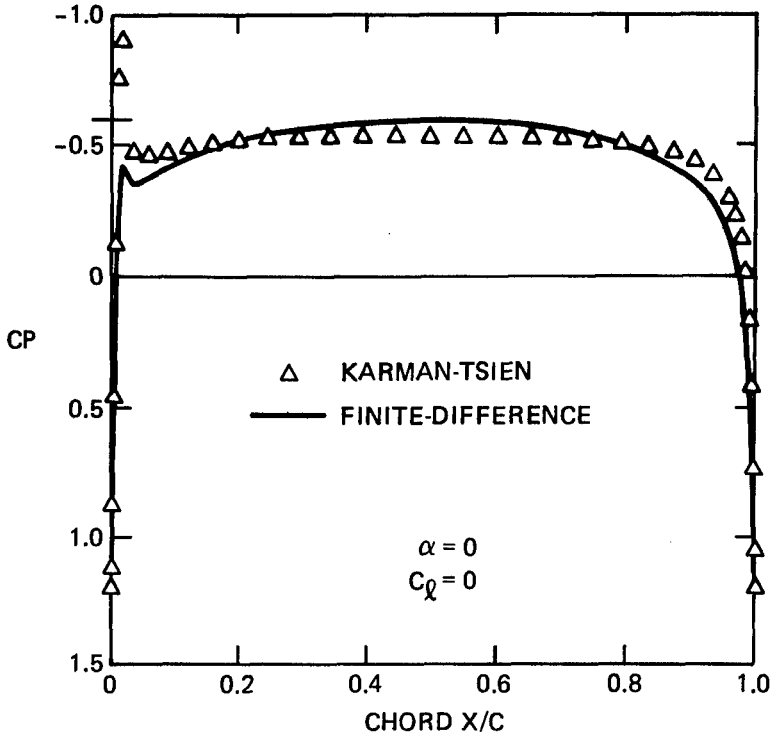

Figure 16a – At Mach 0.750

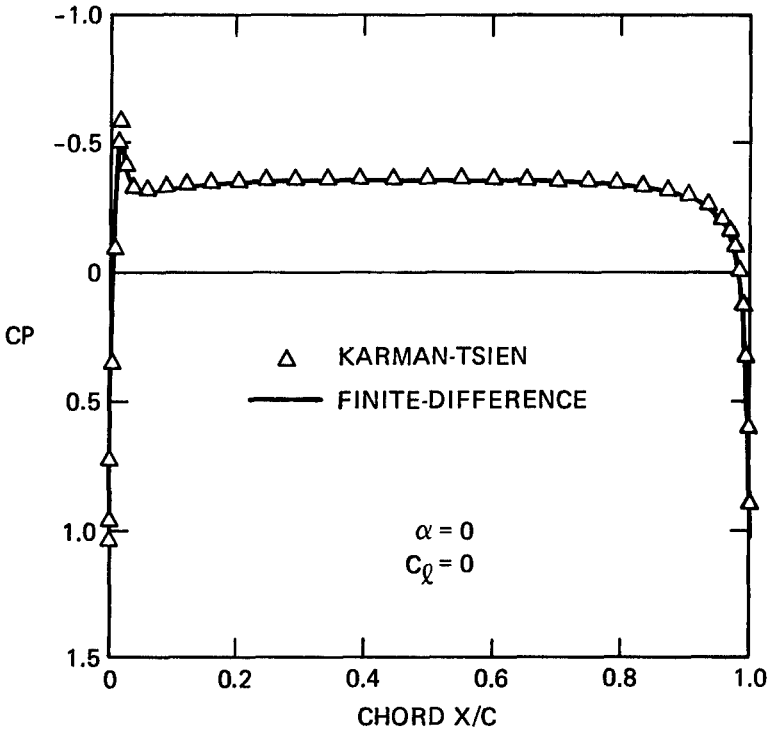

Figure 16b – At Mach 0.400
(Flow condition is well below sonic velocity)

Figure 16 – Comparison of Karman-Tsien Method with Present Results for a 15 Percent Ellipse with Slightly Rounded Leading Edge

ADDITIONAL CASES

Solutions by the present method for the NACA 0012 airfoil are shown in Figure 17 for different lifting conditions. Since the 0012 is analytically described it provides a convenient test case. A circulation control case for a 15-percent ellipse and critical Mach number is presented in Figure 18. Note that even though the angle of attack is negative, the pressure distribution is such that positive lift results from the specified circulation condition.

CONCLUDING REMARKS

The use of compressibility correction factors for estimating critical Mach numbers can lead to misleading results - even for comparisons of different designs. This is attributable to the characteristic overprediction at the leading edge and underprediction near the midchord of suction pressures. Therefore, a comparison of the critical Mach number of airfoils with different types of pressure distributions could lead to false conclusions.

The possibility of extending this basic method to supercritical flow was investigated numerically. The inbedded region of supersonic flow requires the use of one-sided finite difference equations that reflect the hyperbolic nature of the governing equations. (Any attempt to go beyond sonic velocity with the elliptic equations produced severe instabilities.) The discontinuity or shockwave that terminates the supersonic region would hopefully be spread over two or more grid points as a result of truncation errors, thereby producing a continuous flow field for the numerical solution to proceed smoothly. The above concepts were successfully applied by Murman and Cole to the small disturbance equations (Reference 5).

Several changes were made to the subsonic program for this investigation. The radial line matrix method was used in the consideration of propagation direction of transonic disturbances. Rather than sweeping line by line in a single theta direction, the computations were started at the forward stagnation point and continued in the direction of the flow to the trailing edge. At each point a check of the local Mach number was made; if it was greater than unity, the hyperbolic equations were used.

No successful solutions were obtained. Failure occurred shortly after a supersonic region appeared. The mode of failure was that the Mach number ahead of the discontinuity grew steadily to unnatural levels, with the point immediately downstream eventually acquiring a zero or even a negative velocity. A tentative explanation is that the truncation error or "numerical viscosity" in the equation as formulated is not sufficient to smooth out the discontinuity. However, this is only conjecture and no theoretical examination has been made of the suitability of the overall concept for transonic flow solutions.

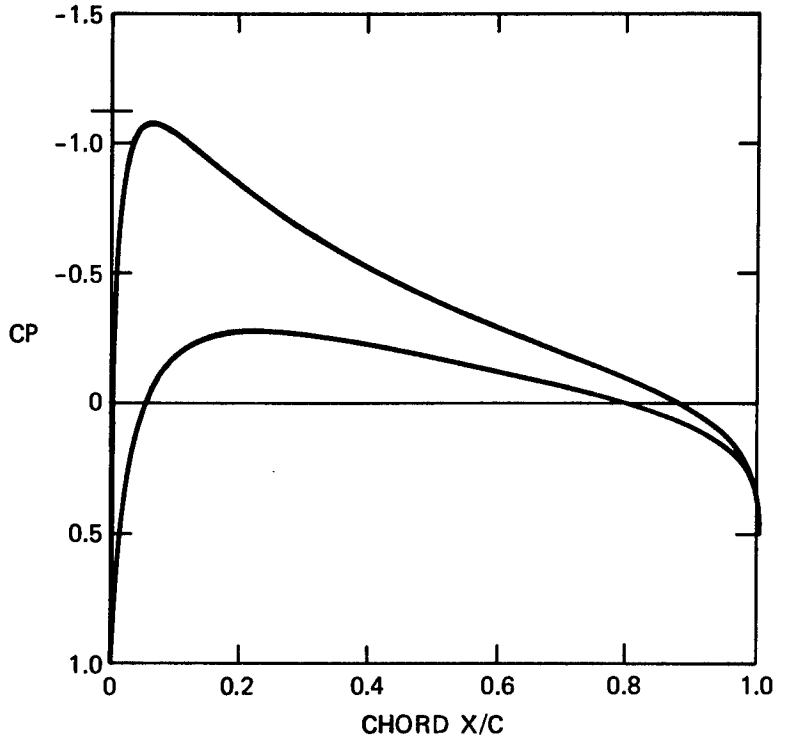

Figure 17a – At M = 0.630, α = 2, C_ℓ = 0.333

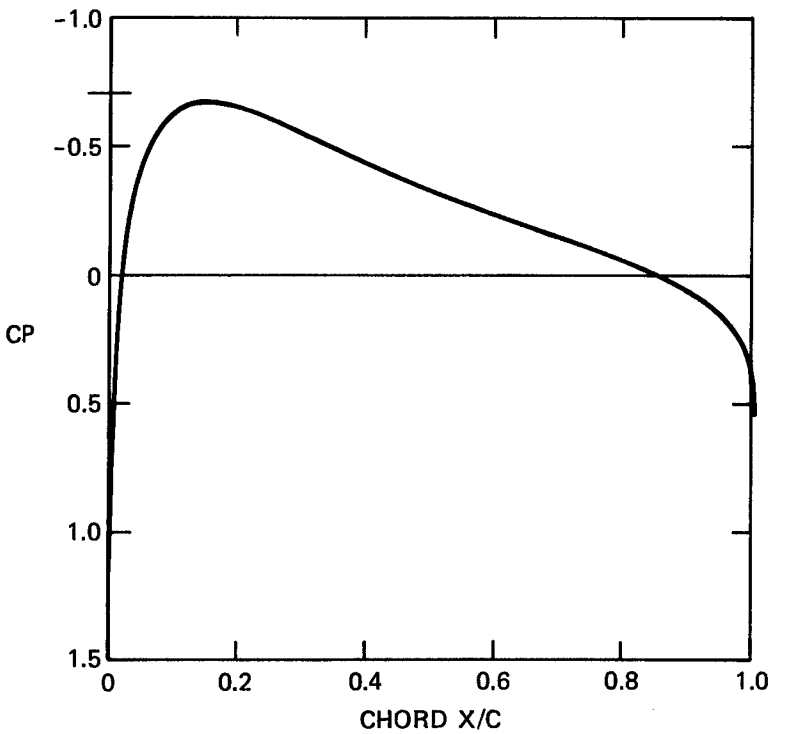

Figure 17b – At M = 0.72, α = 0, C_ℓ = 0

Figure 17 – Present Method Solutions for NACA 0012

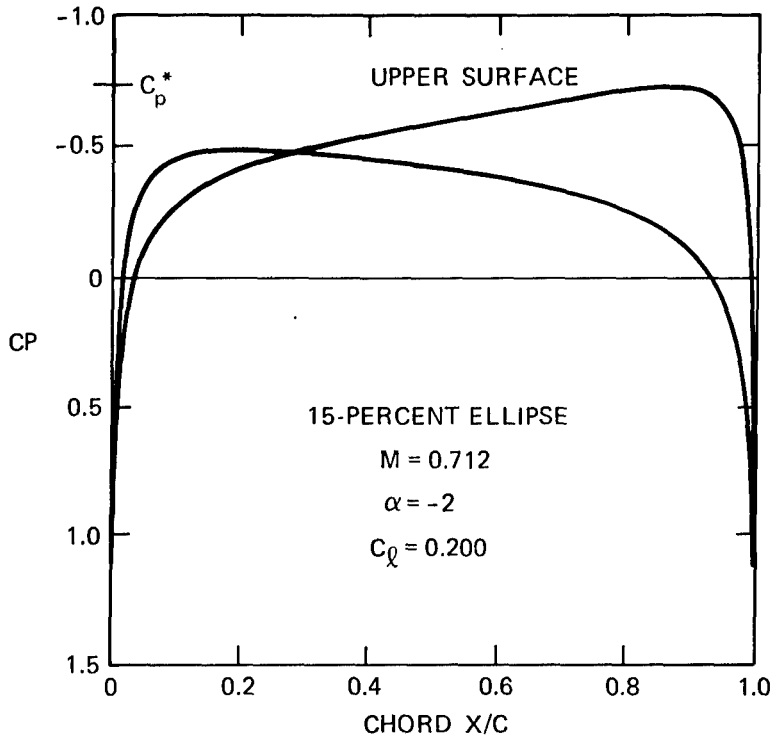

Figure 18 – Circulation Control Case for a 15-Percent Ellipse at Critical Mach Number

APPENDIX
FINITE DIFFERENCE EQUATIONS

Finite difference approximations for the partial derivatives can be obtained from Taylor series expansions. The grid notation of Figure 5 is used to obtain the expansions in the uniform Δr, $\Delta\theta$ mesh:

$$\Phi_\theta = \frac{\Phi_2 - \Phi_4}{2\Delta\theta} - \frac{1}{6}\frac{\partial^3 \Phi}{\partial\theta^3}\bigg|_o (\Delta\theta)^2 + \text{HOT}$$

$$\Phi_{\theta\theta} = \frac{\Phi_2 - 2\Phi_o + \Phi_4}{(\Delta\theta)^2} - \frac{1}{12}\frac{\partial^4 \Phi}{\partial\theta^4}\bigg|_o (\Delta\theta)^2 + \text{HOT}$$

Analogous expressions are obtained for the r derivatives.

The centered differences used are given below; they have a truncation error of order $(\Delta\theta)^2$ or $(\Delta r)^2$ as indicated above.

With

$$c = \frac{1}{m} = \Delta r$$

$$b = \frac{2\pi}{\ell} = \Delta\theta$$

the expressions are:

$$\Phi_r = \frac{\Phi_1 - \Phi_3}{2c}$$

$$\Phi_{rr} = \frac{\Phi_1 - 2\Phi_o + \Phi_3}{c^2}$$

$$\Phi_\theta = \frac{\Phi_2 - \Phi_4}{2b}$$

$$\Phi_{\theta\theta} = \frac{\Phi_2 - 2\Phi_o + \Phi_4}{b^2}$$

$$\rho_r = \frac{\rho_1 - \rho_3}{2c}$$

$$\rho_\theta = \frac{\rho_2 - \rho_4}{2b}$$

These are substituted into the continuity equation (38). Collecting terms and rearranging results in the linear algeraic equation

$$A\Phi_4 + B\Phi_o + C\Phi_2 = D$$

where

$$A = \rho_2 - \rho_4 - 4\rho_o$$

$$B = 8\rho_o \left(\frac{r^2 b^2}{c^2} + 1\right)$$

$$C = \rho_4 - \rho_2 - 4\rho_o$$

$$D = (\rho_4 - \rho_2)\left(\frac{2b}{r}\right)[\sin(\theta + \alpha) + Er] + \frac{b^2}{c^2}(\rho_1 - \rho_3)[r^2(\Phi_1 - \Phi_3)$$

$$- 2c\cos(\theta + \alpha)] + 2\rho_o rc(\Phi_1 - \Phi_3) + 4\rho_o r^2(\Phi_1 + \Phi_3)$$

The boundary conditions at the surface are similarly written in finite difference form. At the trailing edge, the Kutta condition ($\theta = 0$) is

$$E = \frac{\Phi_2 - \Phi_4}{2b} - \sin(\alpha)$$

The complexity of introducing an imaginary external grid line (reflection) for the flow tangency condition can be avoided by using the following one-sided difference formula:

$$\Phi_r = \cos(\theta + \alpha) = -\frac{1}{2c}(4\Phi_o - \Phi_3 - 3\Phi_1)$$

from which there results at $r = 1$

$$\Phi_1 = \frac{4\Phi_o - \Phi_3 + 2c\cos(\theta + \alpha)}{3}$$

REFERENCES

1. Sells, C.C.L., *"Plane Subcritical Flow past a Lifting Aerofoil,"* (Proc. Roy. Soc. A. 308, 1968, pp. 377-401; also RAE Tech Rep 67146).

2. Kacprzynski, J.J., *"Fortran IV Program for the Catherall-Foster-Sells Method for Calculation of the Plane Inviscid Incompressible Flow past a Lifting Aerofoil,"* Ottawa, Canada, Apr 1970. (National Aeronautical Establishment LTR-HA-2).

3. Melnik, R. and D.C. Ives, *"Subcritical Flows over Two-Dimensional Airfoils by a Multistrip Method of Integral Relations,"* Bethpage, N.Y., Oct 1970. 9 p. (Grumman Rpt RE 393J) (AD876 261).

4. Baurdoux, H.I. and J.W. Boerstoel, *"Symmetrical Transonic Potential Flows around Quasi-Elliptical Aerofoil Sections,"* The Netherlands, Dec 1968 (National Aerospace Laboratory NLR-TR 69007U).

5. Murman, E.M. and J.D. Cole, *"Calculation of Plane Steady Transonic Flows,"* New York, Jan 1970. (AIAA paper 70-188).

INITIAL DISTRIBUTION

Copies	
1	USAAMRDL/Ft. Eustis
2	ONR 1 ONR 432 1 ONR 461
1	NRL/Lib 2029
1	USNA/Library
1	NAVPGSCOL/Library
1	NAVAIRDEVCEN/Tech Library
1	NAVWPNCEN/Tech Library
1	NSWC/White Oak Library
1	NAVAIRSYSCOM/AIR 320D
12	DDC
1	USAFFDL/Appl Mech Library
1	AEDC
5	NASA 1 HQS NASA 2 NASA AMES RES CEN 1 Tech Library 1 H. Lomax 2 NASA LANGLEY RES CEN 1 Tech Library 1 J.C. South
3	U MARYLAND 1 W.L. Melnik 1 J.D. Anderson 1 I. Babuska
1	U TENNESSEE SPACE INST/Library
2	U VIRGINIA 1 Alderman Library 1 Engineering Library
1	W VIRGINIA U/Dept Aero Engr
1	ANALYTICAL METHODS INC F. Dvorak
1	BOEING CO/Vertol Div
1	BELL AEROSPACE CORP Bell Helicopter/Ft. Worth
1	DOUGLAS AIRCRAFT/Library

Copies	
1	GENERAL DYNAMICS CONVAIR Library
1	FAIRCHILD-HILLER/Germantown Tech Library
1	FLOW RESEARCH, INC/E. Murman
2	GRUMMAN AEROSPACE 1 Library 1 R.E. Melnik
1	LOCKHEED BURBANK/Library
1	KAMAN AIRCRAFT CORP
1	LING-TEMCO-VOUGHT/Tech Library
1	MCDONNELL-DOUGLAS/LONG BE Library
2	UNITED AIRCRAFT CORP 1 Research Department 1 Sikorsky Aircraft Div

CENTER DISTRIBUTION

Copies	Code	
30	5214.1	Reports Distribution
1	522.1	Library (C)
1	522.2	Library (A)
2	522.3	Aerodynamics Library